JOC Article

Functionalized 2′-Amino-α-L-LNA: Directed Positioning of Intercalators for DNA Targeting

T. Santhosh Kumar,[†] Andreas S. Madsen,[†] Michael E. Østergaard,[‡] Sujay P. Sau,[‡] Jesper Wengel,[†] and Patrick J. Hrdlicka*,[‡]

Nucleic Acid Center, Department of Physics and Chemistry, University of Southern Denmark, DK-5230 Odense M, Denmark, and Department of Chemistry, University of Idaho, Moscow, Idaho 83844-2343

hrdlicka@uidaho.edu

Received September 18, 2008

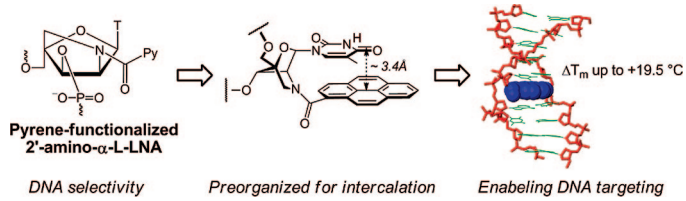

Chemically modified oligonucleotides are increasingly applied in nucleic acid based therapeutics and diagnostics. LNA (locked nucleic acid) and its diastereomer α-L-LNA are two promising examples thereof that exhibit increased thermal and enzymatic stability. Herein, the synthesis, biophysical characterization, and molecular modeling of N2′-functionalized 2′-amino-α-L-LNA is described. Chemoselective N2′-functionalization of protected amino alcohol **1** followed by phosphitylation afforded a structurally varied set of target phosphoramidites, which were incorporated into oligodeoxyribonucleotides. Incorporation of pyrene-functionalized building blocks such as 2′-*N*-(pyren-1-yl)carbonyl-2′-amino-α-L-LNA (monomer **X**) led to extraordinary increases in thermal affinity of up to +19.5 °C per modification against DNA targets in particular. In contrast, incorporation of building blocks with small nonaromatic N2′-functionalities such as 2′-*N*-acetyl-2′-amino-α-L-LNA (monomer **V**) had detrimental effects on thermal affinity toward DNA/RNA complements with decreases of as much as −16.5 °C per modification. Extensive thermal DNA selectivity, favorable entropic contributions upon duplex formation, hybridization-induced bathochromic shifts of pyrene absorption maxima and increases in circular dichroism signal intensity, and molecular modeling studies suggest that pyrene-functionalized 2′-amino-α-L-LNA monomers **W**−**Y** having short linkers between the bicyclic skeleton and the pyrene moiety allow high-affinity hybridization with DNA complements and precise positioning of intercalators in nucleic acid duplexes. This rigorous positional control has been utilized for the development of probes for emerging therapeutic and diagnostic applications focusing on DNA targeting.

Introduction

Oligonucleotides are widely used for modulation of gene expression (e.g., antigene/antisense/siRNA),[1] for detection of nucleic acid targets,[2] and as building blocks of novel self-assembling biomaterials.[3] Chemical modification of oligonucleotides is often required to provide adequate protection from enzymatic degradation, to facilitate strong binding to complementary nucleic acid targets, and to add functionality to oligonucleotides. Incorporation of conformationally restricted nucleotide monomers into oligonucleotides is a popular approach toward this end.[4,5] Locked nucleic acid (LNA, *β*-D-*ribo* con-

[†] University of Southern Denmark.
[‡] University of Idaho.

(1) (a) Duca, M.; Vekhoff, P.; Oussedik, K.; Halby, L.; Arimondo, P. B. *Nucleic Acids Res.* **2008**, *36*, 5123–5138. (b) Simon, P.; Cannata, F.; Concordet, J.-P.; Giovannangeli, C. *Biochimie* **2008**, *90*, 1109–1116. (c) Kurreck, J. *Eur. J. Biochem.* **2003**, *270*, 1628–1644. (d) Corey, D. R. *J. Clin. Invest.* **2007**, *117*, 3615–3622. (e) Watts, J. K.; Deleavey, G. F.; Damha, M. J. *Drug Discovery Today* **2008**, *13*, 842–855.

(2) (a) Asseline, U. *Curr. Opin. Chem.* **2006**, *10*, 491–518. (b) Ranasinghe, R. T.; Brown, T. *Chem. Commun.* **2005**, 5487–5502.

(3) (a) Wengel. J *Org. Biomol. Chem.* **2004**, *2*, 277–280. (b) Gothelf, K. V.; LaBean, T. H. *Org. Biomol. Chem.* **2005**, *3*, 4023–4037. (c) Clever, G. H.; Kaul, C.; Carell, T. *Angew. Chem., Int. Ed.* **2007**, *46*, 6226–6236.

(4) For reviews, see: (a) Meldgaard, M.; Wengel, J *J. Chem. Soc. Perkin Trans. 1* **2000**, *353*, 9–3554. (b) Leumann, C. J *Bioorg. Med. Chem.* **2002**, *10*, 841–854.

10.1021/jo802037v CCC: $40.75
Published on Web 12/24/2008

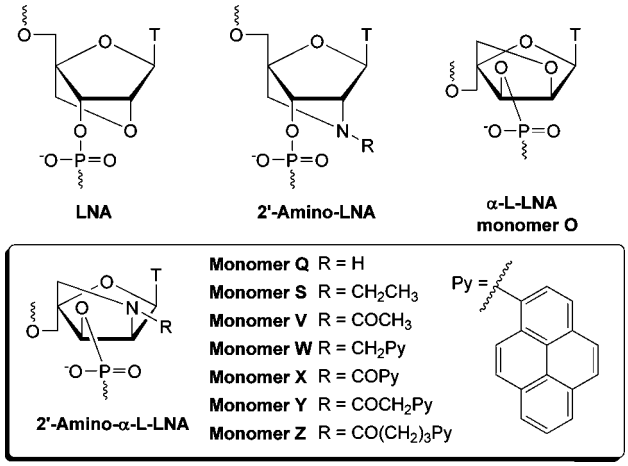

FIGURE 1. Structures of LNA, 2′-amino-LNA, α-L-LNA (monomer **O**), and 2′-amino-α-L-LNA monomers **Q**−**Z**.

figuration, Figure 1) is a very promising member of this class of compounds. LNA[6−8] exhibits increases in thermal affinity toward DNA/RNA complements of up to +10 °C per modification along with markedly improved enzymatic stability relative to that of unmodified oligodeoxyribonucleotides (ONs).[9,10] These properties render LNA with pronounced therapeutic and diagnostic potential,[11−14] which is underlined by ongoing phase I/II clinical evaluations of LNA drug candidates against a variety of diseases. One of the diastereoisomers of LNA, i.e., α-L-LNA[6,15] (α-L-*ribo* configuration, monomer **O**, Figure 1), shares the beneficial properties of LNA and has been used as antisense ONs,[16−18] triplex-forming ONs,[19] modified DNAzymes,[20] and transcription factor decoy ONs.[21]

We have previously taken advantage of the known high-affinity hybridizations of 2′-amino-LNA[6,22] (Figure 1) to develop a series of N2′-functionalized 2′-amino-LNAs, which precisely position functional entities in the minor groove of nucleic acid duplexes without compromising duplex stability.[23] This has resulted in the development of tools for applications within therapeutics, diagnostics, and material science, including (a) probes yielding brightly fluorescent duplexes upon hybridization to DNA/RNA targets with quantum yields approaching unity,[23d,k] (b) probes for single nucleotide polymorphism (SNP) detection,[23b,h] (c) nucleic acid architectures autosignaling their self-assembly,[23b,h] and (d) artificial dinuclear ribonucleases.[23j]

Stimulated by these findings, we recently developed a synthetic route to 2′-amino-α-L-LNA (α-L-*ribo* configuration, monomer **Q**, Figure 1)[6,24] and N2′-functionalized analogs thereof (Figure 1). Appended functional entities were anticipated to be positioned in the major groove of nucleic acid duplexes.[24a] However, initial studies with N2′-pyrene-functionalized 2′-amino-α-L-LNA suggest that the conjugated functional entity is directed toward the duplex core instead.[25,26] This has already resulted in the development of promising tools for DNA targeting,[25a] detection of single nucleotide polymorphisms,[25b] and nucleic acid structural engineering.[25d]

Herein, full experimental details on the synthesis of a structurally varied set of N2′-functionalized 2′-amino-α-L-LNA phosphoramidites and their incorporation into ONs are presented (Figure 1). Results from biophysical and computational studies

(5) For recent representative examples, see: (a) Morita, K.; Takagi, M.; Hasegawa, C.; Kaneko, M.; Tsutsumi, S.; Sone, J.; Ishikawa, T.; Imanishi, T.; Koizumi, M. *Bioorg. Med. Chem.* **2003**, *11*, 2211–2226. (b) Albaek, N.; Petersen, M.; Nielsen, P. *J. Org. Chem.* **2006**, *71*, 7731–7740. (c) Honcharenko, D.; Vargese, O. P.; Plashkevych, O.; Barman, J.; Chattopadhyaya, J. *J. Org. Chem.* **2006**, *71*, 299–314. (d) Varghese, O. P.; Barman, J.; Pathmasiri, W.; Plaskevych, O.; Honcharenko, D.; Chattopadhyaya, J. *J. Am. Chem. Soc.* **2006**, *128*, 15173–15187. (e) Hari, Y.; Obika, S.; Ohnishi, R.; Eguchi, K.; Osaki, T.; Ohishi, H.; Imanishi, T. *Bioorg. Med. Chem.* **2006**, *14*, 1029–1038. (f) Plashkevych, O.; Chatterjee, S.; Honcharenko, D.; Pathmasiri, W.; Chattopadhyaya, J. *J. Org. Chem.* **2007**, *72*, 4716–4726. (g) Srivastava, P.; Barman, J.; Pathmasiri, W.; Plaskevych, O.; Wenska, M.; Chattopadhyaya, J. *J. Am. Chem. Soc.* **2007**, *129*, 8362–8379. (h) Sabatino, D.; Damha, M. J. *J. Am. Chem. Soc.* **2007**, *129*, 8259–8270. (i) Abdur Rahman, S. M.; Seki, S.; Obika, S.; Yoshikawa, H.; Miyashita, K.; Imanishi, T. *J. Am. Chem. Soc.* **2008**, *130*, 4886–4896. (j) Enderlin, G.; Nielsen, P. *J. Org. Chem.* **2008**, *73*, 6891–6894.

(6) We define LNA, α-L-LNA, 2′-amino-LNA, and 2′-amino-α-L-LNA as a oligonucleotide containing one or more 2′-*O*,4′-*C*-methylene-β-D-ribofuranosyl monomer(s), 2′-*O*,4′-*C*-methylene-α-L-ribofuranosyl monomer(s), 2′-amino-2′-deoxy-2′-*N*,4′-*C*-methylene-β-D-ribofuranosyl monomer(s), or 2′-amino-2′-deoxy-2′-*N*,4′-*C*-methylene-α-L-ribofuranosyl monomer(s), respectively. Similar definitions are used for N2′-functionalized α-L-LNA derivatives.

(7) (a) Singh, S. K.; Nielsen, P.; Koshkin, A. A.; Wengel, J. *Chem. Commun.* **1998**, 455–456. (b) Koshkin, A. A.; Singh, S. K.; Nielsen, P.; Rajwanshi, V. K.; Kumar, R.; Meldgaard, M.; Olsen, C. E.; Wengel, J. *Tetrahedron* **1998**, *54*, 3607–3630. (c) Wengel, J. *Acc. Chem. Res.* **1999**, *32*, 301–310.

(8) Obika, S.; Nanbu, D.; Hari, Y.; Andoh, J.; Morio, K.; Doi, T.; Imanishi, T. *Tetrahedron Lett.* **1998**, *39*, 5401–5404.

(9) Petersen, M.; Wengel, J. *Trends Biotechnol.* **2003**, *21*, 74–81.

(10) Kaur, H.; Babu, B. R.; Maiti, S. *Chem. Rev.* **2007**, *107*, 4672–4697.

(11) Jepsen, J. S.; Wengel, J. *Curr. Opin. Drug Discovery Dev.* **2004**, *7*, 188–194.

(12) Frieden, M.; Ørum, H. *IDrugs* **2006**, *9*, 706–711.

(13) Grünweller, A; Hartmann, R. K. *Biodrugs* **2007**, *21*, 235–243.

(14) Stenvang, J.; Silahtaroglu, A. N.; Lindow, M.; Elmen, J.; Kauppinen, S. *Sem. Cancer Biol.* **2008**, *18*, 89–102.

(15) (a) Rajwanshi, V. K.; Håkansson, A. E.; Dahl, B. M.; Wengel, J. *Chem. Commun.* **1999**, 1395–1396. (b) Sørensen, M. D.; Kværnø, L.; Bryld, T.; Håkansson, A. E.; Verbeure, B.; Gaubert, G.; Herdewijn, P.; Wengel, J. *J. Am. Chem. Soc.* **2002**, *124*, 2164–2176.

(16) Arzumanov, A.; Stetsenko, D. A.; Malakhov, A. D.; Techelt, S.; Sørensen, M. D.; Babu, B. R.; Wengel, J.; Gait, M. J. *Oligonucleotides* **2003**, *13*, 435–453.

(17) Frieden, M.; Christen, S. M.; Mikkelsen, N. D.; Rosenbohm, C.; Thrue, C. A.; Westergaard, M.; Hansen, H. F.; Ørum, H.; Koch, T. *Nucleic Acids Res.* **2003**, *31*, 6365–6372.

(18) Fluiter, K.; Frieden, M.; Vreijling, J.; Rosenbohm, C.; De Wissel, M. B.; Christensen, S. M.; Koch, T.; Ørum, H.; Baas, F. *ChemBioChem* **2005**, *6*, 1104–1109.

(19) Kumar, N.; Nielsen, K. E.; Maiti, S.; Petersen, M. *J. Am. Chem. Soc.* **2006**, *128*, 14–15.

(20) Vester, B.; Hansen, L. H.; Lundberg, L. B.; Babu, B. R.; Sørensen, M. D.; Wengel, J.; Doubtwaite, S. *BMC Mol. Biol.* **2006**, *7*, 19.

(21) Crinelli, R.; Bianchi, M.; Gentilini, L.; Palma, L.; Sørensen, M. D.; Bryld, T.; Babu, B. R.; Arar, K.; Wengel, J.; Magnani, M. *Nucleic Acids Res.* **2004**, *32*, 1874–1885.

(22) Singh, S. K.; Kumar, R.; Wengel, J. *J. Org. Chem.* **1998**, *63*, 10035–10039.

(23) (a) Sørensen, M. D.; Petersen, M.; Wengel, J. *Chem. Commun.* **2003**, 2130–2131. (b) Hrdlicka, P. J.; Babu, B. R.; Sørensen, M. D.; Wengel, J. *Chem. Commun.* **2004**, 1478–1479. (c) Babu, B. R.; Hrdlicka, P. J.; McKenzie, C. J.; Wengel, J. *Chem. Commun.* **2005**, 1705–1707. (d) Hrdlicka, P. J.; Babu, B. R.; Sørensen, M. D.; Harrit, N.; Wengel, J. *J. Am. Chem. Soc.* **2005**, *127*, 13293–13299. (e) Lindegaard, D.; Babu, B. R.; Wengel, J. *Nucleosides Nucleotides Nucleic Acids* **2005**, *24*, 679–681. (f) Bramsen, J. B.; Laursen, M. B.; Damgaard, C. K.; Lena, S. W.; Babu, B. R.; Wengel, J.; Kjems, J. *Nucleic Acids Res.* **2007**, *35*, 5886–5897. (g) Kalek, M.; Madsen, A. S.; Wengel, J. *J. Am. Chem. Soc.* **2007**, *129*, 9392–9400. (h) Umemoto, T.; Hrdlicka, P. J.; Babu, B. R.; Wengel, J. *ChemBioChem* **2007**, *8*, 2240–2248. (i) Lindegaard, D.; Madsen, A. S.; Astakhova, I. V.; Malakhov, A. D.; Babu, B. R.; Korshun, V. A.; Wengel, J. *Bioorg. Med. Chem.* **2008**, *16*, 94–99. (j) Kalek, M.; Benediktson, P.; Vester, B.; Wengel, J. *Chem. Commun.* **2008**, 762–764. (k) Østergaard, M. E.; Maity, J.; Wengel, J.; Hrdlicka, P. J. Abstracts of Papers, 235th ACS National Meeting (2008), New Orleans, BIOL-032.

(24) (a) Hrdlicka, P. J.; Kumar, T. S.; Wengel, J. *Nucleosides Nucleotides Nucleic Acids* **2005**, *24*, 1101–1104. (b) Kumar, T. S.; Madsen, A. S.; Wengel, J.; Hrdlicka, P. J. *J. Org. Chem.* **2006**, *71*, 4188–4201.

(25) (a) Hrdlicka, P. J.; Kumar, T. S.; Wengel, J. *Chem. Commun.* **2005**, 4279–4281. (b) Kumar, T. S.; Wengel, J.; Hrdlicka, P. J. *ChemBioChem* **2007**, *8*, 1122–1125. (c) Andersen, N. K.; Wengel, J.; Hrdlicka, P. J. *Nucleosides Nucleotides Nucleic Acids* **2007**, *26*, 1415–1417. (d) Kumar, T. S.; Madsen, A. S.; Østergaard, M. E.; Wengel, J.; Hrdlicka, P. J. *J. Org. Chem.* **2008**, *73*, 7060–7066.

(26) Preliminary results have been briefly outlined in Kumar, T. S.; Madsen, A. S.; Wengel, J.; Hrdlicka, P. J. *Nucleosides Nucleotides Nucleic Acids* **2007**, *26*, 1403–1405.

SCHEME 1. Synthesis of N2′-Functionalized 2′-Amino-α-L-LNA Phosphoramidites[a]

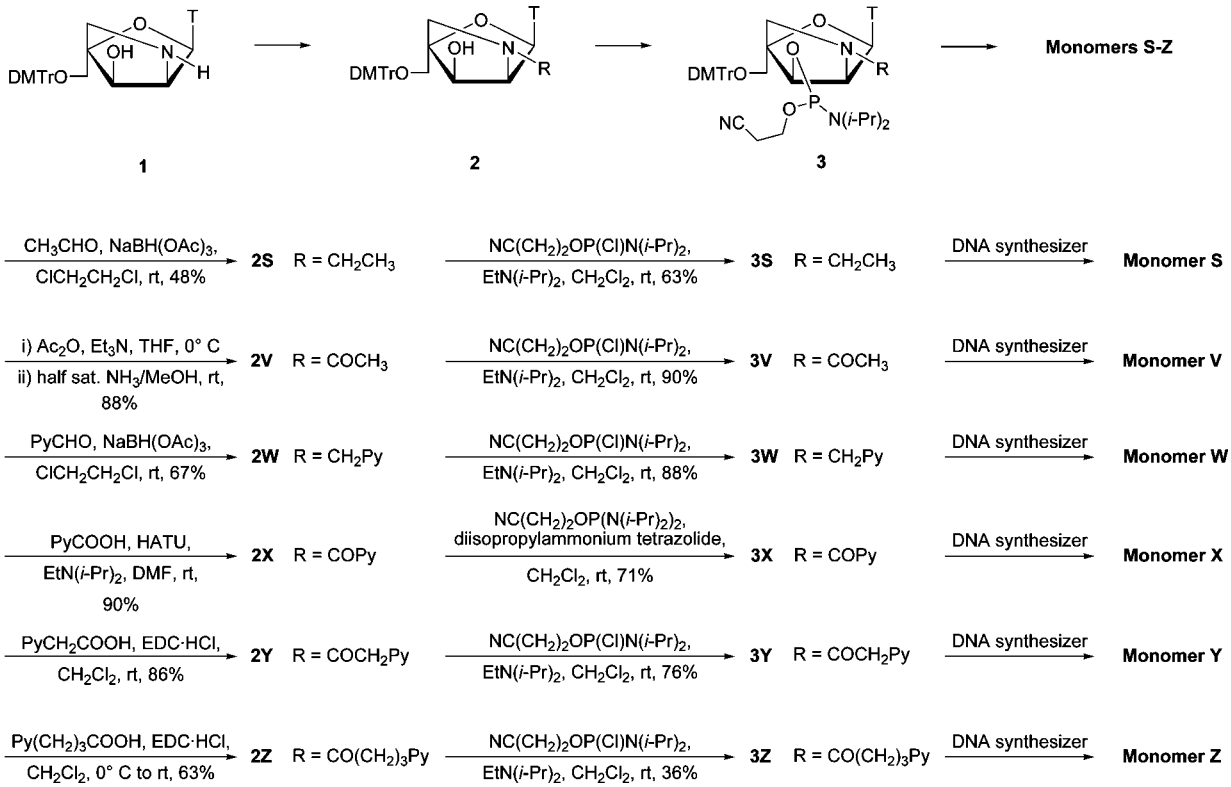

[a] DMTr = 4,4′-dimethoxytrityl, T = thymin-1-yl, Py = pyren-1-yl, EDC·HCl = 1-ethyl-3-(3-dimethylaminopropyl)-carbodiimide hydrochloride, HATU = *O*-(7-azabenzotriazole-1-yl)-*N*,*N*,*N*′,*N*′-tetramethyluronium hexafluorophosphate.

are discussed together with the suggested binding mode of the appended functional entities.

Results and Discussion

Synthesis of N2′-Functionalized 2′-Amino-α-L-LNA. Known O5′-tritylated bicyclic nucleoside **1**,[24b] which is obtained from commercially available diacetone-α-D-glucose in 5% overall yield over 17 steps involving eight chromatographic purification steps, was used as a suitable starting material for the synthesis of N2′-functionalized 2′-amino-α-L-LNA phosphoramidites **3Q**−**3Z** (Scheme 1). The targets were selected to probe the available structural space in nucleic acid duplexes and fall into two groups based on the nature of the N2′-moiety, i.e., monomers with small nonaromatic units (monomers **Q**, **S**, and **V**) or with aromatic units (monomers **W**−**Z**). Sodium triacetoxyborohydride mediated reductive amination[27] of secondary amine **1** with acetaldehyde or 1-pyrenecarbaldehyde furnished tertiary amines **2S** and **2W**[25a] in 48% and 67% yield, respectively. Chemoselective N-acylation of amino alcohol **1** was achieved using two different strategies. Treatment of nucleoside **1** with slight excess of acetic anhydride followed by selective O3′-deacylation using dilute methanolic ammonia furnished nucleoside **2V** in excellent 88% yield over two steps. EDC-mediated coupling of amino alcohol **1** with 1-pyrenylcarboxylic acid, 1-pyrenylacetic acid, or 4-(1-pyrenyl)butyric acid afforded nucleosides **2X**, **2Y**,[25b,d] and **2Z** in 62%, 86%, and 63% yield, respectively. A HATU (*O*-(7-azabenzotriazole-1-yl)-*N*,*N*,*N*′,*N*′-tetramethyluronium hexafluorophosphate)-mediated coupling procedure successfully improved the yield of **2X** to 90%. Disappearance of ^{1}H NMR signals of the exchangeable 3′-OH protons upon D_2O addition ascertained the N2′-functionalized constitution of nucleosides **2S**−**2Z**, which subsequently were converted to the corresponding phosphoramidites **3S**−**3Z** using 2-cyanoethyl *N*,*N*′-(diisopropyl)-phosphoramidochloridite and Hünig's base. While amidites **3S**−**3Y** were obtained in good to excellent yields (60−90%), **3Z** was only obtained in 36% yield. The yield of **3X** was improved using bis(*N*,*N*-diisopropylamino)-2-cyanoethoxyphosphine in dichloromethane with diisopropylammonium tetrazolide[28] as activator (71%).

Synthesis of ONs was performed in 0.2 μmol scale using an automated DNA synthesizer. The corresponding phosphoramidites for incorporation of α-L-LNA thymine monomer **O** (obtained from commercial sources) and 2′-amino-α-L-LNA thymine monomer **Q** (synthesized via a known protocol)[24b] were incorporated into our preferred model system, i.e., a set of mixed sequence 9-mer ONs, as previously described.[15b,24b] Standard procedures were applied for incorporation of N2′-functionalized 2′-amino-α-L-LNA thymine monomers **S**−**Z** (Figure 1) except for extended coupling times: **3S** (10 min), **3V** (10 min), **3W**[25a] (30 min), **3Y**[25b] (30 min), **3X** (30 min), and **3Z** (15 min)) using 1*H*-tetrazole as catalyst resulting in stepwise coupling yields of ∼99% for monomers **S**, **V**, **X**, **Y**, and **Z** and ∼95% for monomer **W** (Figure 1 for structures). Following standard workup and purification, the composition and purity (>80%) of all modified ONs was verified by MALDI-MS (Table S3, Supporting Information)[29] and ion-exchange HPLC, respectively. Please note that the unmodified reference DNA and RNA strands are denoted **D1/D2** and **R1/R2**, respectively, and ONs

(27) Abdel-Magid, A. F.; Carson, K. G.; Harris, B. D.; Maryanoff, C. A.; Shah, R. D. *J. Org. Chem.* **1996**, *61*, 3849–3862.

(28) Pedersen, D. S.; Rosenbohm, C.; Koch, T. *Synthesis* **2002**, 802–808.

(29) See Supporting Information.

TABLE 1. Thermal Denaturation Data for N2′-Functionalized 2′-Amino-α-L-LNA and Reference Strands against DNA Complements[a]

			T_m [ΔT_m/mod] (°C)								
ON	duplex	**B** =	T	**O**	**Q**	**S**	**V**	**W**	**X**	**Y**	**Z**
B1	5′-G**B**G ATA TGC		28.5	31.0 [+2.5]	26.5 [−2.0]	20.0 [−8.5]	17.5 [−11.0]	35.5 [+7.0]	38.5 [+10.0]	39.0 [+10.5]	29.0 [+0.5]
D2	3′-CAC TAT ACG										
B2	5′-GTG A**B**A TGC		28.5	34.5 [+6.0]	29.0 [+0.5]	20.0 [−8.5]	16.5 [−12.0]	42.5 [+14.0]	47.5 [+19.0]	44.0 [+15.5]	34.5 [+6.0]
D2	3′-CAC TAT ACG										
B3	5′-GTG ATA **B**GC		28.5	31.5 [+3.0]	27.5 [−1.0]	16.5 [−12.0]	14.5 [−14.0]	39.0 [+10.5]	42.5 [+14.0]	40.0 [+11.5]	ND
D2	3′-CAC TAT ACG										
D1	5′-GTG ATA TGC		28.5	32.0 [+3.5]	28.0 [−0.5]	17.0 [−11.5]	12.0 [−16.5]	35.0 [+6.5]	39.0 [+10.5]	38.5 [+10.0]	29.0 [+0.5]
B4	3′-CAC **B**AT ACG										
D1	5′-GTG ATA TGC		28.5	36.5 [+8.0]	31.0 [+2.5]	22.5 [−6.0]	19.0 [−9.5]	44.0 [+15.5]	48.0 [+19.5]	45.0 [+16.5]	35.0 [+6.5]
B5	3′-CAC TA**B** ACG										
D1	5′-GTG ATA TGC		28.5	36.0 [+3.8]	27.5 [−0.5]	<10	<10	ND	53.5 [+12.5]	55.5 [+13.5]	ND
B6	3′-CAC **B**A**B** ACG										
B7	5′-G**B**G A**B**A **B**GC		28.5	36.0 [+2.5]	27.0 [−0.5]	<10	<10	ND	ND	69.0 [+13.5]	ND
D2	3′-CAC TAT ACG										

[a] Thermal denaturation temperatures [T_m values in °C (ΔT_m = change in T_m value calculated relative to **D1**:**D2**, **D1**:**R2**, and **R1**:**D2** reference duplexes)] measured as the maximum of the first derivative of the melting curve (A_{260} vs temperature) recorded in medium salt buffer ($[Na^+]$ = 110 mM, $[Cl^-]$ = 100 mM, pH 7.0 (NaH_2PO_4/Na_2HPO_4)), using 1.0 μM concentrations of the two complementary strands. T_m values are averages of at least two measurements; A = adenin-9-yl DNA monomer, C = cytosin-1-yl DNA monomer, G = guanin-9-yl DNA monomer, T = thymin-1-yl DNA monomer, **O** = α-L-LNA thymin-1-yl monomer (Figure 1). For structures of monomers **O**−**Z** see Figure 1. ND = not determined.

TABLE 2. Thermal Denaturation Data for N2′-Functionalized 2′-Amino-α-L-LNA and Reference Strands against RNA Complements[a]

			T_m [ΔT_m/mod] (°C)								
ON	duplex	**B** =	T	**O**	**Q**	**S**	**V**	**W**	**X**	**Y**	**Z**
B1	5′-G**B**G ATA TGC		26.5	32.5 [+6.0]	27.5 [+1.0]	19.5 [−7.0]	19.0 [−7.5]	27.0 [+0.5]	32.5 [+6.0]	32.5 [+6.0]	26.5 [±0]
R2	3′-CAC UAU ACG										
B2	5′-GTG A**B**A TGC		26.5	35.0 [+8.5]	28.5 [+2.0]	18.5 [−8.0]	17.0 [−9.5]	31.5 [+5.0]	36.5 [+10.0]	36.0 [+9.5]	33.5 [+7.0]
R2	3′-CAC UAU ACG										
B3	5′-GTG ATA **B**GC		26.5	32.0 [+5.5]	28.0 [+1.5]	19.0 [−7.5]	16.5 [−10.0]	28.0 [+1.5]	33.5 [+7.0]	32.5 [+6.0]	ND
R2	3′-CAC UAU ACG										
R1	5′-GUG AUA UGC		24.5	31.0 [+6.5]	27.5 [+3.0]	19.5 [−5.0]	17.5 [−7.0]	23.5 [−1.0]	29.0 [+4.5]	30.5 [+6.0]	19.5 [−5.0]
B4	3′-CAC **B**AT ACG										
R1	5′-GUG AUA UGC		24.5	34.5 [+10.0]	29.0 [+4.5]	21.5 [−3.0]	20.5 [−4.0]	32.0 [+7.5]	36.0 [+11.5]	36.5 [+12.0]	31.0 [+6.5]
B5	3′-CAC TA**B** ACG										
R1	5′-GUG AUA UGC		24.5	35.5 [+5.5]	28.5 [+2.0]	<10	<10	ND	39.0 [+7.3]	44.0 [+9.8]	ND
B6	3′-CAC **B**A**B** ACG										
B7	5′-G**B**G A**B**A **B**GC		26.5	44.0 [+5.8]	31.0	<10	<10	ND	ND	52.5 [+8.7]	ND
D2	3′-CAC UAU ACG										

[a] For conditions of thermal denaturation experiments see Table 1.

containing a single incorporation of a modified nucleotide in the 5′-G**B**G ATA TGC context are named **O1**, **Q1**, **S1**, etc. Similar conventions were used for ONs in the **B2**−**B7** series (Tables 1 and 2). In addition, the following descriptive nomenclature is used: α-L-amino-LNA (**Q**-series), Et-α-L-amino-LNA (**S**-series), Ac-α-L-amino-LNA (**V**-series), PyMe-α-L-amino-LNA (**W**-series), PyCO-α-L-amino-LNA (**X**-series), PyAc-α-L-amino-LNA (**Y**-series), and PyBu-α-L-amino-LNA (**Z**-series).

Thermal Denaturation Studies. Experimental Setup. The effect upon incorporation of one to three **O**−**Z** monomers (Figure 1) into mixed sequence 9-mer ONs on thermal affinity toward DNA and RNA targets (Tables 1 and 2, respectively) was evaluated by UV thermal denaturation experiments using medium salt buffer ($[Na^+]$ = 110 mM) and compared to unmodified DNA. The UV thermal denaturation curves of all modified duplexes exhibited sigmoidal monophasic transitions with hyperchromicities (9−15%) that are comparable to the corresponding unmodified DNA:DNA or DNA:RNA duplexes (Figure S1, Supporting Information).[29] All changes in thermal denaturation temperatures (T_m) of modified nucleic acid duplexes are discussed relative to T_m values of unmodified reference duplexes unless otherwise mentioned. In addition, the Watson−Crick specificity of ONs with a single central incorporation of monomer **O**−**Z** (**B2**-series) was evaluated by determining T_m values of the duplexes with DNA/RNA strands with central mismatches (Table 3).

Thermal Denaturation Studies. α-L-LNA and 2′-Amino-α-L-LNA. Reference ONs. α-L-LNAs **O1**−**O5** exhibit substantially increased thermal affinity toward DNA (ΔT_m up to +8.0 °C, Table 1) and RNA complements (ΔT_m = up to +10.0 °C, Table 2). The corresponding 2′-amino-α-L-LNAs **Q1**−**Q5** display notably smaller increases in thermal affinity (ΔT_m up to +2.5 °C with DNA, Table 1; ΔT_m up to +4.5 °C with RNA, Table 2). Similar ΔT_m values for duplexes between α-L-amino-LNA **Q4** and DNA/RNA complements determined at different ionic strengths were observed (Table S4, Supporting Information),[29] suggesting that the 2-oxo-5-azabicyclo[2.2.1]heptane

TABLE 3. Discrimination of Mismatched DNA/RNA Targets by N2′-Functionalized 2′-Amino-α-L-LNA

			T_m [ΔT_m] (°C)							
			DNA: 3′-CAC T**B**T ACG				RNA: 3′-CAC U**B**U ACG			
ON	sequence	**B** =	A	C	G	T	A	C	G	U
D1	5′-GTG ATA TGC		**28.5**	12.0 [−16.5]	19.0 [−9.5]	11.5 [−17.0]	**26.5**	<10 [<−16.5]	22.0 [−4.5]	<10 [<−16.5]
O2	5′-GTG A**O**A TGC		**34.5**	13.0 [−21.5]	21.5 [−13.0]	14.5 [−20.0]	**35.0**	14.0 [−21.0]	28.5 [−6.5]	14.5 [−20.5]
Q2	5′-GTG A**Q**A TGC		**29.0**	<10 [<−19.0]	17.5 [−11.5]	<10 [<−19.0]	**28.5**	<10 [<−18.5]	22.5 [−6.0]	<10 [<−18.5]
S2[b]	5′-GTG A**S**A TGC		**28.5**	<10 [<−18.5]	17.0 [−11.5]	<10 [<−18.5]	**27.0**	<10 [<−17.0]	25.5 [−1.5]	<10 [<−17.0]
V2[b]	5′-GTG A**V**A TGC		**24.5**	<10 [<−14.5]	14.5 [−10.0]	<10 [<−14.5]	**24.5**	<10 [<−14.5]	28.0 [+3.5]	<10 [<−14.5]
W2	5′-GTG A**W**A TGC		**42.5**	30.0 [−12.5]	37.0 [−5.5]	39.0 [−3.5]	**31.5**	19.5 [−12.0]	30.5 [−1.0]	27.0 [−4.5]
X2	5′-GTG A**X**A TGC		**47.5**	31.0 [−16.5]	40.0 [−7.5]	40.5 [−7.0]	**36.5**	21.0 [−15.5]	33.5 [−3.0]	28.5 [−8.0]
Y2	5′-GTG A**Y**A TGC		**44.0**	26.0 [−18.0]	38.5 [−5.5]	34.0 [−10.0]	**36.0**	14.5 [−21.5]	33.0 [−3.0]	25.0 [−11.0]
Z2	5′-GTG A**Z**A TGC		**34.5**	17.0 [−17.5]	20.0 [−14.5]	20.0 [−14.5]	**33.5**	<10 [<−22.5]	17.5 [−16.0]	<10 [<−22.5]

[a] For conditions of thermal denaturation experiments see Table 1. T_m values of fully matched duplexes are shown in bold. ΔT_m = change in T_m value relative to fully matched DNA:DNA or DNA:RNA duplex. [b] T_m values for duplexes involving **S2** and **V2** are measured using high salt buffer ([Na^+] = 710 mM, [Cl^-] = 100 mM, pH 7.0 (NaH_2PO_4/Na_2HPO_4)).

skeleton of monomer **Q** is not protonated at physiological pH. The increased binding affinity of α-L-LNA and 2′-amino-α-L-LNA was accompanied by improved discrimination of singly mismatched DNA and RNA targets relative to unmodified DNA **D1** (e.g., ΔT_m values for α-L-amino-LNA **Q2** and **D1** against DNA mismatches, Table 3).

Thermal Denaturation Studies. N2′-Pyrene-Functionalized 2′-Amino-α-L-LNA. Incorporation of a single PyMe/PyCO/PyAc-α-L-amino-LNA monomer **W**, **X** or **Y**, respectively, into ONs resulted in extraordinary increases in thermal affinity toward DNA complements (ΔT_m from +6.5 to +19.5 °C, Table 1). Moderate increases were observed upon incorporation of PyBu-α-L-amino-LNA monomer **Z** (ΔT_m up to +6.5 °C, Table 1). The observed trends in thermal affinity of singly modified strands toward DNA targets (**X** > **Y** > **W** ≫ **Z**) suggest that (a) alkanoyl linkers are thermally preferred over alkyl linkers of the same length (**X** > **W**), and (b) shorter linkers are thermally preferred (**X** > **Y** ≫ **Z**). For a discussion on the sequence-dependent variations of T_m values observed for these ONs, the reader is directed to Supporting Information.[29] Interestingly, additive increases in thermal affinity toward DNA targets are observed upon multiple incorporations of PyAc-α-L-amino-LNA **Y** monomers (e.g., compare T_m/mod values of **Y6**:**D1**, **Y4**:**D1**, and **Y5**:**D1**, Table 1), whereas subadditive increases are observed for the corresponding α-L-LNA **O6**, 2′-amino-α-L-LNA **Q6**, or PyMe-α-L-amino-LNA **X6**. Thus, PyAc-α-L-amino-LNA monomer **Y** lends itself as the building block of choice for applications necessitating densely functionalized ONs with maximal thermal affinity toward DNA targets.

PyCO/PyAc-α-L-amino-LNAs (**X1**-**X6** and **Y1**-**Y7**, respectively) exhibit prominent and additive increases in thermal affinity toward RNA complements (ΔT_m from +4.5 to +12.0 °C, Table 2). In contrast, minor destabilizations to moderate increases were observed for PyMe/PyBu-α-L-amino-LNAs **W1**-**W5** and **Z1**-**Z5**, respectively, with the exception of **Z4**, which exhibited a very pronounced decrease in thermal affinity toward its RNA target (Table 2).

Accordingly, N2′-pyrene-functionalized 2′-amino-α-L-LNA exhibit a marked DNA selectivity, i.e., a positive $\Delta\Delta T_m$/mod (DNA-RNA) = ΔT_m/mod (DNA) − ΔT_m/mod (RNA). This is particularly noteworthy as the parent α-L-LNA and 2′-amino-α-L-LNA exhibit moderate RNA selectivity ($\Delta\Delta T_m$/mod (DNA-RNA) = −3.5 to −1.7 °C, Tables 1 and 2 or, more conveniently, Table S5, Supporting Information[29]). PyMe/PyCO-α-L-amino-LNAs exhibit the most pronounced DNA selectivity ($\Delta\Delta T_m$/mod (DNA-RNA) = +6.0 to +9.0 °C, Table S5, Supporting Information), suggesting that short linkers between the pyrene and nucleoside moieties facilitate DNA selectivity. Although PyMe/PyCO-α-L-amino-LNAs exhibit a similar degree of DNA selectivity as acyclic intercalating nucleic acids (INAs),[30] 2′-*O*-pyrenylmethyl uridines,[31] or pyrene-functionalized 4′-*C*-piperazinomethyl thymidines,[32] they generally form stronger duplexes with DNA targets, which renders them as highly interesting probes for DNA-targeting applications.[25a]

Centrally modified PyMe-α-L-amino-LNAs **W2** exhibit less efficient discrimination of mismatched DNA/RNA targets than the corresponding reference strand **D1** (Table 3). Interestingly, a change in linker chemistry from methylene to carbonyl (**W** → **X**) results in higher affinity toward DNA/RNA complements as well as significantly improved mismatch discrimination (Table 3). With the exception of T:T/U mismatches, PyCO-α-L-amino-LNA **X2** displays mismatch discrimination comparable to that of reference strand **D1**. Increases in linker length result in progressively improved discrimination of DNA/RNA mismatches (compare ΔT_m data for **X2**, **Y2**, and **Z2**, Table 3). Accordingly, PyBu-α-L-amino-LNA **Z2** exhibits superior discrimination of RNA mismatches in general and of the challenging T:rG mismatch in particular (ΔT_m = −16.0 °C, data for **Z2**, Table 3), relative to the already highly discriminative α-L-LNA **O2**.

Thermal Denaturation Studies. N2′-Ethyl/Acetyl-Modified 2′-Amino-α-L-LNA. Et-α-L-amino-LNAs **S1**−**S7** exhibit greatly decreased thermal affinities toward DNA/RNA targets in general and complementary DNA in particular (ΔT_m/mod down to −12.0 °C, Table 1). These effects are even more pronounced with Ac-α-L-amino-LNAs **V1**−**V7**, which exhibit decreases in T_m values down to −16.5 °C per modification (Table 1). Accordingly, no duplex transitions could be observed for ONs with two or three incorporations of **S** or **V** monomers and their DNA/RNA targets. Interestingly, the large decreases in thermal affinity toward DNA/RNA complements of Et/Ac-α-L-amino-LNA generally did not compromise Watson−Crick specificity (see data for **S2** and **V2**, Table 3), which suggests that base-pairing is preserved.

It is noteworthy that an exchange of a centrally positioned PyCO-α-L-amino-LNA monomer **X** with a corresponding Ac-

(30) (a) Christensen, U. B.; Pedersen, E. B. *Nucleic Acids Res.* **2002**, *30*, 4918–4925. (b) Filichev, V. V.; Hilmy, K. M. H.; Christensen, U. B.; Pedersen, U. B. *Tetrahedron Lett.* **2004**, *45*, 4907–4910.
(31) Yamana, K.; Iwase, R.; Furutani, S.; Tsuchida, H.; Zako, H.; Yamaoka, T.; Murakami, A. *Nucleic Acids Res.* **1999**, *27*, 2387–2392.
(32) Bryld, T.; Højland, T.; Wengel, J. *Chem. Commun.* **2004**, 1064–1065.

TABLE 4. Energetics Derived from Thermal Denaturation Curves of Duplexes between 2′-Amino-α-L-LNA Functionalized with Nonaromatic Moieties and DNA/RNA[a]

		complementary DNA			complementary RNA		
ON	sequence	ΔG^{298} [$\Delta\Delta G^{298}$] (kJ/mol)	ΔH [$\Delta\Delta H$] (kJ/mol)	$T^{298}\Delta S$ [$\Delta(T^{298}\Delta S)$] (kJ/mol)	ΔG^{298} [$\Delta\Delta G^{298}$] (kJ/mol)	ΔH [$\Delta\Delta H$] (kJ/mol)	$T^{298}\Delta S$ [$\Delta(T^{298}\Delta S)$] (kJ/mol)
D1	5′-GTG ATATGC	−41	−327	−286	−38	−275	−237
O2	5′-GTGA**O**ATGC	−46 [−5]	−354[−27]	−308[−22]	−46[−8]	−361[−86]	−315[−78]
Q2	5′-GTGA**Q**ATGC	*−41 [0]*	*−312[+15]*	*−271[+15]*	*−40[−2]*	*−302[−27]*	*−261[−24]*
S2	5′-GTG A**S**ATGC	−33 [+8]	−349[−22]	−316[−30]	−31[+7]	−352[−77]	−321[−84]
V2	5′-GTGA**V**ATGC	*−29[+12]*	*−295[+32]*	*−266[+20]*	−30[+8]	−303[−28]	−273[−36]

[a] Thermal denaturation curves were obtained as described in Tables 1 and 2. $\Delta\Delta G^{298}$, $\Delta\Delta H$, and $\Delta(T^{298}\Delta S)$, change in ΔG^{298}, ΔH and $(T^{298}\Delta S)$ values, respectively, calculated relative to **D1**:**D2** and **D1**:**R2** reference duplexes). Values in italics indicate deviation from (or lack of) monomer trend. ND = not determined. See Table S6 in Supporting Information for data from **B1**−**B5** series.

α-L-amino-LNA monomer **V** (i.e., a formal change of pyrene to methyl) was accompanied by a decrease in thermal affinity toward complementary DNA of 31.0 °C (compare T_m values of **X2**:**D2** and **V2**:**D2**, Table 1). This suggests very different binding modes for ONs modified with monomers **S/V** and **W/Y**, respectively, which was underlined upon additional biophysical characterization (vide infra).

Additional Biophysical Characterization of N2′-Functionalized 2′-Amino-α-L-LNA. Experimental Setup. To obtain additional insight into the highly divergent thermal affinities of N2′-functionalized 2′-amino-α-L-LNA, the following biophysical studies were performed: (a) determination of thermodynamic parameters for duplex formation, (b) CD spectra, (c) UV−vis spectra (shifts of pyrene absorption maxima), and (d) molecular modeling studies.

Thermodynamic parameters for duplex formation were determined by melting curve analysis assuming bimolecular reactions and two-state equilibrium hypothesis. Quality of the baseline permitting, thermodynamic parameters for two melting curves per investigated duplex were determined, and an average value is listed. In full agreement with expectations, formation of all studied duplexes was favorable ($\Delta G^{298} < 0$ kJ/mol), with favorable enthalpic ($\Delta H < 0$ kJ/mol) and unfavorable entropic contributions ($T^{298}\Delta S < 0$ kJ/mol). The thermodynamic data rely on assumptions of two-state melting behavior and a heat capacity change $\Delta C_p = 0$ upon hybridization, which may not necessarily be fulfilled. However, apart from few exceptions (see footnote *a* in Table 4), the observed enthalpic/entropic contributions for hybridization of N2′-functionalized 2′-amino-α-L-LNA to DNA/RNA targets clearly followed monomer- and sequence-specific trends, which validates the utilized approach (data shown for the representative **B2**-series in Tables 4 and 5; for data and full discussion of **B1**−**B5** series see Table S6, Supporting Information[29]).

Duplexes between N2′-functionalized 2′-amino-α-L-LNA and DNA/RNA complements were studied by force field simulations. For this, DNA duplexes were built in silico and modified with an N2′-functionalized 2′-amino-α-L-LNA monomer. A starting B-type helix geometry was chosen as duplexes between α-L-LNA and DNA complements adopt helix geometries that are globally unperturbed relative to unmodified DNA:DNA duplexes.[33] ONs with centrally positioned modifications (**B2**-series) were selected for the simulations to minimize the influence of fraying on the helix geometry near the modified nucleotides. The position of N2′-functionalities was explored using a truncated Monte Carlo search,[29] and the partially constrained duplexes were subjected to stochastic dynamics simulations using the all-atom AMBER force field[34] and GB/SA solvation model[35] as implemented in the MacroModel V9.1 suite of programs.[36]

Integrated Structural Discussion. α-L-LNA and 2′-Amino-α-L-LNA. Reference ONs. The markedly increased thermal affinity of α-L-LNAs **O1**−**O5** toward DNA/RNA relative to unmodified ONs results from a more favorable enthalpic term that largely is counterbalanced by an unfavorable entropic term, i.e., $\Delta\Delta G_{298}(\mathbf{O2_{DNA}}) = \Delta G_{298}(\mathbf{O2}:\mathbf{D2}) - \Delta G_{298}(\mathbf{D1}:\mathbf{D2}) = -5$ kJ/mol; $\Delta\Delta H(\mathbf{O2_{DNA}}) = \Delta H(\mathbf{O2}:\mathbf{D2}) - \Delta H(\mathbf{D1}:\mathbf{D2}) = -27$ kJ/mol; $\Delta(T^{298}\Delta S)$ $(\mathbf{O2_{DNA}}) = T^{298}\Delta S$ $(\mathbf{O2}:\mathbf{D2}) - T^{298}\Delta S$ $(\mathbf{D1}:\mathbf{D2}) = -22$ kJ/mol (Table 4). This suggests that high thermal affinity of the conformationally restricted α-L-LNAs **O1**−**O5** toward DNA/RNA complements is a result of a more favorable stacking/hydrogen bonding geometry and/or duplex solvation rather than preorganization of the single stranded probe.

Similarly, the hybridization of 2′-amino-α-L-LNAs **Q1**−**Q5** to complementary RNA is also driven by favorable enthalpy that is partially counterbalanced by unfavorable entropy, although the individual contributions are less pronounced than for α-L-LNAs **O1**−**O5** (e.g., $\Delta\Delta H = -86$ and -27 kJ/mol for $\mathbf{O2_{RNA}}$ and $\mathbf{Q2_{RNA}}$, respectively, Table 4). The energetics for hybridization of **Q1**−**Q5** to DNA complements are sequence-dependent and could not be fitted to a clear pattern (Tables 4 and S6, Supporting Information[29]).

The applied molecular modeling protocol successfully reproduced expected global and local features of α-L-LNA duplex **O2**:**D2** (Figure S4, Supporting Information), providing credibility to the applied computational protocol. These features of **O2**:**D2** include a standard B-type global duplex geometry similar to that of **D1**:**D2** (Figure S3, Supporting Information) and very characteristic local perturbations in the backbone needed to accommodate the inverted configurations at the C2′-, C3′- and C4′-positions of α-L-LNA monomer **O**.[29,33] Interestingly, the global helix structures of **O2**:**D2** and **Q2**:**D2** (Figure S5, Supporting Information)[29] are virtually identical, which is validated by very similar circular dichroism spectra of **Q7**:**D2** and **O7**:**D2** (Figure S2, Supporting Information). Thus, different solvation patterns rather than substantially altered helical geometries likely account for the diverging energetics observed

(33) Nielsen, K. M. E.; Petersen, M.; Håkansson, A. E.; Wengel, J.; Jacobsen, J. P. *Chem. Eur. J.* **2002**, *8*, 3001–3009.

(34) (a) Weiner, S. J.; Kollman, P. A.; Case, D. A.; Singh, U. C.; Ghio, C.; Alagona, G.; Profeta, S.; Weiner, P. *J. Am. Chem. Soc.* **1984**, *106*, 765–784. (b) Weiner, S. J.; Kollman, P. A.; Nguyen, D. T.; Case, D. A. *J. Comput. Chem.* **1986**, *7*, 230–252.

(35) Still, W. C.; Tempczyk, A.; Hawley, R. C.; Hendrickson, T. *J. Am. Chem. Soc.* **1990**, *112*, 6127–6129.

(36) *MacroModel*, version 9.1, S; LLC: New York, NY, 2005.

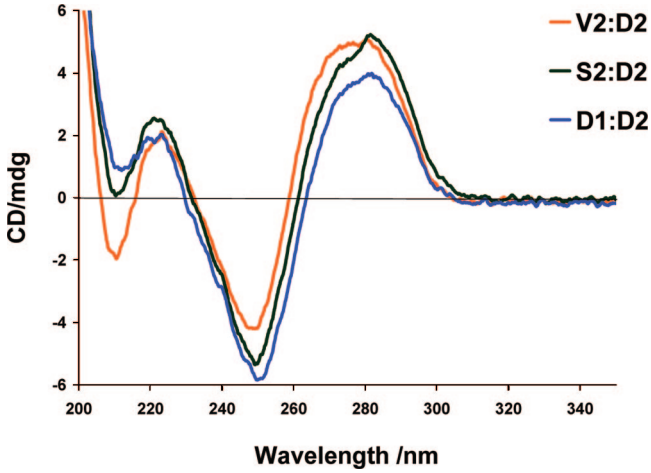

FIGURE 2. Circular dichroism spectra of **D1**:**D2**, **S2**:**D2**, and **V2**:**D2**.

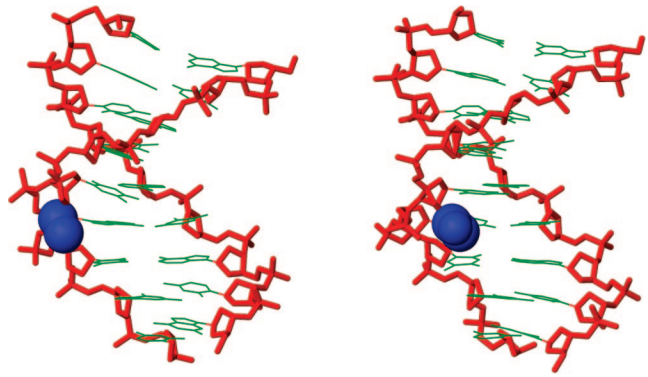

FIGURE 3. Side view representations of the lowest energy structure of **S2**:**D2** (left) and **V2**:**D2** (right). For clarity, hydrogen atoms, sodium ions and bond orders have been omitted. Coloring scheme: nucleobases, green; sugar−phosphate backbone, red; ethyl moiety of monomer **S** and acetyl moiety of monomer **V**, blue.

for these closely related ONs upon hybridization with DNA/RNA complements.

Integrated Structural Discussion. N2′-Ethyl/Acetyl-Modified 2′-Amino-α-L-LNA. The dramatically destabilized duplexes between Et/Ac-α-L-amino-LNAs and DNA/RNA targets ($\Delta\Delta G^{298}$ up to +12 kJ/mol) result from unfavorable entropic components that are only partially counterbalanced by favorable enthalpic components (e.g., $\Delta(T^{298}\Delta S)(\mathbf{S2_{RNA}}) = -84$ kJ/mol and $\Delta\Delta H(\mathbf{S2_{RNA}}) = -77$ kJ/mol, Table 4).

Intriguingly, very similar CD spectra are observed for **S2**:**D2**, **V2**:**D2**, and the reference duplex **D1**:**D2** suggesting that incorporation of **S** and **V** monomers renders these duplexes globally unperturbed while dramatically lowering stability (Figure 2). In accordance with this, the lowest energy structures of Et-α-L-amino-LNA duplex **S2**:**D2** (Figures 3 and S6, Supporting Information) and Ac-α-L-amino-LNA duplex **V2**:**D2** (Figures 3 and S7, Supporting Information) globally resembled each other and α-L-amino-LNA duplex **Q2**:**D2** (Figure S5, Supporting Information).[29] In **S2**:**D2** the ethyl group of $\mathbf{S_5}$ protrudes from the major groove valley to become involved in a steric clash with H5′ of $\mathbf{A_6}$ (for numbering scheme see Figure 4). We speculate that unfavorable desolvation of the apolar ethyl moiety (whereby fewer water molecules are released) and interference with structural water along the sugar −phosphate backbone,[37,38] in a similar manner as proposed for

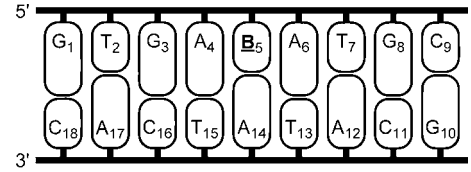

FIGURE 4. Nucleotide numbering for duplexes studied by molecular modeling; **B** = thymidine (**D1**) or monomers **O**−**Z** (**O2**−**Z2**).

monomer **Q**,[29] accounts for the unfavorable entropy observed upon hybridization of Et-α-L-amino-LNA **S2** with DNA/RNA targets (Table 4). In a related manner, one part of the N2′-acetyl moiety of monomer **V** (i.e., either the -CO- or $-CH_3$) in **V2**:**D2** is directed toward the major groove where it can interfere with structural water, while the other part simultaneously protrudes into the duplex core to disrupt $\pi-\pi$ stacking (Figures 3 and S7, Supporting Information).[29]

To sum up, biophysical characterization and computer simulations jointly suggest that N2′-functionalization of 2′-amino-α-L-LNA, contrary to preliminary expectations,[24a] is not suitable to position small nonaromatic moieties in the major groove of duplexes with DNA or RNA complements.

Integrated Structural Discussion. N2′-Pyrene-Functionalized 2′-Amino-α-L-LNA. The very pronounced stabilization of duplexes between PyMe-α-L-amino-LNA or PyAc-α-L-amino-LNA and complementary DNA (e.g., $\Delta\Delta G_{298}(\mathbf{W2_{DNA}}) = -12$ kJ/mol) results from highly favorable entropy (e.g., $\Delta\Delta(T^{298}\Delta S)(\mathbf{W2_{DNA}}) = +32$ kJ/mol, Table 5). Stabilization of duplexes between PyCO-α-L-amino-LNA and DNA targets (e.g., $\Delta\Delta G^{298}(\mathbf{X2_{DNA}}) = -18$ kJ/mol) is to a greater extent driven by favorable enthalpic factors. The moderate stabilization of duplexes between PyBu-α-L-amino-LNA and DNA complements (e.g., $\Delta\Delta G^{298}(\mathbf{Z2_{DNA}}) = -5$ kJ/mol) originates from favorable enthalpy contributions that mostly were counterbalanced by unfavorable entropy components ($\Delta\Delta H(\mathbf{Z2_{DNA}}) = -9$ kJ/mol, $\Delta(T^{298}\Delta S)(\mathbf{Z2_{DNA}}) = -4$ kJ/mol, Table 5).

The observed stabilization of duplexes between PyMe/PyCO/PyAc-α-L-amino-LNA with RNA complements results from favorable enthalpy ($\Delta\Delta H = -53$, -68, and -58 kJ/mol for $\mathbf{W2_{RNA}}$, $\mathbf{X2_{RNA}}$, and $\mathbf{Y2_{RNA}}$, respectively). However, comparison with 2′-amino-α-L-LNA reference strands instead of unmodified DNA suggests that entropic contributions also aid duplex formation with RNA targets (e.g., $\Delta(T^{298}\Delta S) = -17$, -28, -17, and -51 kJ/mol for $\mathbf{W3_{RNA}}$, $\mathbf{X3_{RNA}}$, $\mathbf{Y3_{RNA}}$, and $\mathbf{Q3_{RNA}}$, respectively, Table S6, Supporting Information).[29]

Thus, energetics suggest that N2′-pyrene-functionalized 2′-amino-α-L-LNAs exhibit binding modes that rely on preorganization, unlike 2′-amino-α-L-LNA modified with nonaromatic moieties.

The pronounced DNA selectivity of PyMe/PyCO/PyAc-α-L-amino-LNA suggests intercalation of the pyrene moieties as a likely binding mode.[30−32,39] The CD spectra of PyAc-α-L-amino-LNA and duplexes with DNA/RNA support this hypothesis as induced CD bands in the region of pyrene absorption (λ = 320−360 nm, Figure 5), a feature indicative of intercalation,[40] are observed upon hybridization. In addition, marked bathochromic shifts of pyrene absorption maxima of ONs containing monomers **W**−**Y** upon hybridization with DNA/RNA targets

(37) Egli, M.; Tereshko, V.; Teplova, M.; Minasov, G.; Joachimiak, A.; Sanishvili, R.; Weeks, C. M.; Miller, R.; Maier, M. A.; An, H.; Cook, P. D.; Manoharan, M. *Biopolymers* **1998**, *48*, 234–252.
(38) Kielkopf, C. L.; Ding, S.; Kuhn, P.; Rees, D. C. *J. Mol. Biol.* **2000**, *296*, 787–801.

TABLE 5. Energetics Derived from Thermal Denaturation Curves of Duplexes between N2′-Pyrene-Functionalized 2′-Amino-α-L-LNA and DNA/RNA[a]

		complementary DNA			complementary RNA		
ON	sequence	ΔG^{298} [$\Delta\Delta G^{298}$] (kJ/mol)	ΔH [$\Delta\Delta H$] (kJ/mol)	$T^{298}\Delta S$ [$\Delta(T^{298}\Delta S)$] (kJ/mol)	ΔG^{298} [$\Delta\Delta G^{298}$] (kJ/mol)	ΔH [$\Delta\Delta H$] (kJ/mol)	$T^{298}\Delta S$ [$\Delta(T^{298}\Delta S)$] (kJ/mol)
D1	5′-GTG ATATGC	−41	−327	−286	−38	−275	−237
W2	5′-GTGA**W**ATGC	−53[−12]	−307[+20]	−254[+32]	−44 [−6]	−328[−53]	−284[−47]
X2	5′-GTG A**X**ATGC	−59[−18]	−348[−21]	−289 [−3]	−49[−11]	−343[−68]	−294[−57]
Y2	5′-GTG A**Y**ATGC	−54[−13]	−321 [+6]	−267[+19]	−48[−10]	−333[−58]	−285[−48]
Z2	5′-GTG A**Z**ATGC	−46 [−5]	−336 [−9]	−290 [−4]	ND	ND	ND

[a] See Table 4 for conditions.

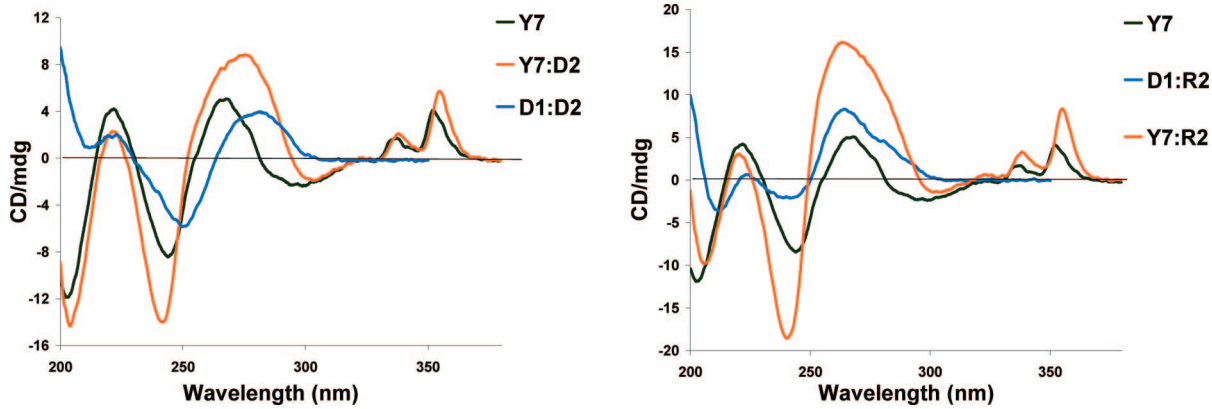

FIGURE 5. Circular dichroism of spectra of **Y7** (5′-G**Y**G A**Y**A **Y**GC) and its duplexes with DNA/RNA complements and reference DNA:DNA (**D1**:**D2**) and DNA:RNA (**D1**:**R2**).

TABLE 6. Pyrene Absorption Maxima for Single-Stranded Pyrene-Functionalized 2′-Amino-α-L-LNA and the Corresponding Duplexes with DNA/RNA Complements[a]

			λ_{max} [$\Delta\lambda_{max}$] (nm)										
	B =	W			X			Y			Z		
ON	sequence	ss	+DNA	+RNA	ss	+DNA	+RNA	ss	+DNA	+RNA	ss	+DNA	+RNA
B1	5′-G**B**G ATA TGC	348	350 [+2]	349 [+1]	349	351 [+2]	351 [+2]	350	351 [+1]	352 [+2]	346	348 [+2]	348 [+2]
B2	5′-GTG A**B**A TGC	347	351 [+4]	349 [+2]	348	353 [+5]	351 [+3]	346	351 [+5]	351 [+5]	346	347 [+1]	346 [±0]
B3	5′-GTG ATA **B**GC	348	351 [+3]	350 [+2]	350	354 [+4]	351 [+1]	348	351 [+3]	351 [+3]	ND	ND	ND
B4	3′-CAC **B**AT ACG	348	350 [+2]	348 [±0]	348	351 [+3]	349 [+1]	350	351 [+1]	351 [+1]	346	347 [+1]	346 [±0]
B5	3′-CAC TA**B** ACG	348	350 [+2]	349 [+1]	348	351 [+3]	351 [+3]	346	351 [+5]	352 [+6]	346	348 [+2]	347 [+1]

[a] Measurements were performed at room temperature on a spectrophotometer in the 300−400 nm range, using a quartz optical cell with a 1.0 cm path length and the same conditions as for thermal denaturation experiments.

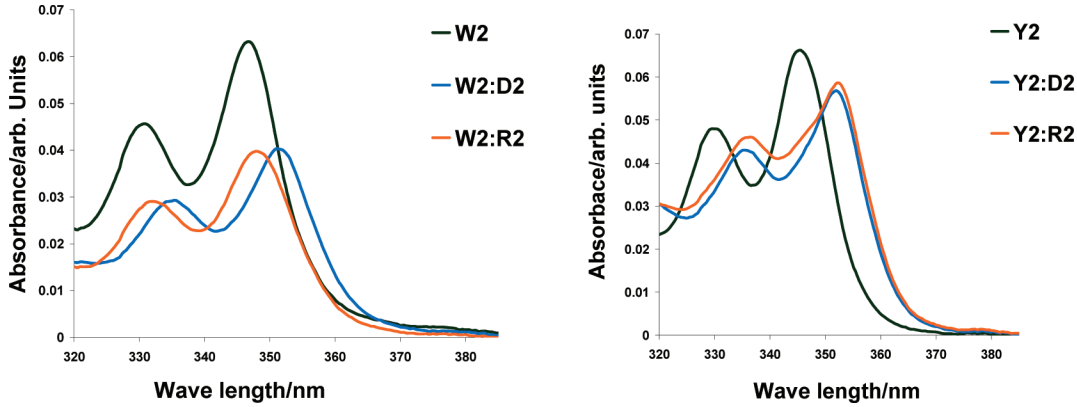

FIGURE 6. Absorption spectra of **W2** (left panel) and **Y2** (right panel) and their duplexes with complementary DNA (**D2**) and RNA (**R2**) targets.

($\Delta\lambda_{max}$ = 1−5 and 0−6 nm, respectively, Table 6) along with hypochromic shifts (illustrated for **W2** and **Y2**, Figure 6) suggest strong electronic interactions between the pyrene and nucleobase moieties in duplexes.[40−42] A change in linker chemistry from alkyl to alkanoyl (PyMe-α-L-amino-LNA **W** → PyCO-α-L-amino-LNA **X**) resulted in small but consistently larger hybrid-

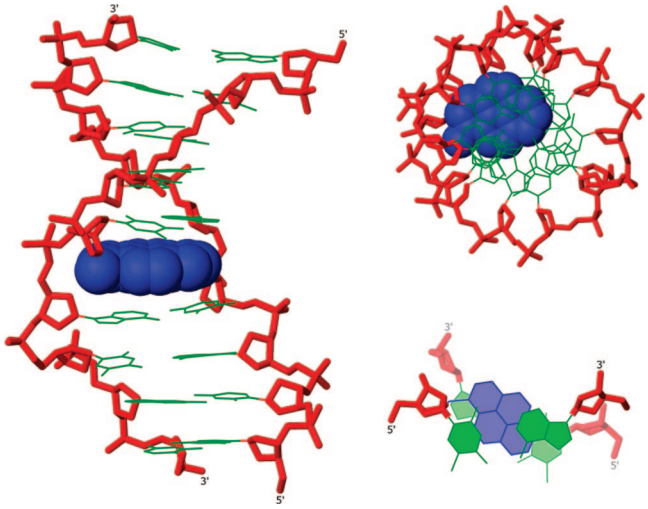

FIGURE 7. Three representations of the lowest energy structure of **W2**:**D2**; side view (left), top view (upper right), and truncated top view showing $\mathbf{W_5A_6}$:$\mathbf{T_{13}A_{14}}$ (lower right). Coloring scheme as in Figure 3 except that pyren-1-yl-methyl moiety of monomer **W** is in blue.

ization-induced bathochromic shifts, and further extension of the alkanoyl linker (PyCO-α-L-amino-LNA **X** → PyAc-α-L-amino-LNA **Y** → PyBu-α-L-amino-LNA **Z**) progressively reversed this trend. The very subtle hybridization-induced bathochromic shifts of pyrene absorption maxima observed with PyBu-α-L-amino-LNA indicate a nonintercalating binding mode of the pyrene moiety of monomer **Z** (Table 6).

In full agreement with biophysical data, the lowest energy structure of the duplex between PyMe-α-L-amino-LNA **W2** and complementary DNA **D2** suggests precise intercalation of the pyrene moiety (Figure 7). It is imperative to stress that the utilized simulation protocol did not initiate from a structure where the pyrene moiety was intercalated, i.e., the pyrene moiety moved from an extrahelical to an intercalated position during the simulation. As expected[43] significant global unwinding, concomitant lengthening of the duplex, and widening of the minor groove was observed upon intercalation. The pyrene moiety forms extensive $\pi-\pi$ stacks with the nucleobase moieties of $\mathbf{W_5}$ and the 3′-flanking $\mathbf{A_6}$ and to a lesser extent with the nucleobase moieties of $\mathbf{T_{13}}$ and $\mathbf{A_{14}}$. The pseudorotational phase angle P and glycosidic torsion angle χ[44] of PyMe-α-L-amino-LNA monomer **W** change little relative to the 2′-amino-α-L-LNA monomer in **Q2**:**D2**. However, P and χ of the adjacent $\mathbf{A_6}$ moiety increase markedly in response to intercalation (P from 97° to 127° and χ from −147° to −105°, for **Q2**:**D2** and **W2**:**D2**, respectively, Tables S7 and S8, Supporting Information),[29] to facilitate efficient $\pi-\pi$ stacking between the pyrene and nucleobase moieties.

The lowest energy structures of duplexes between PyCO-α-L-amino-LNA **X2** or PyAc-α-L-amino-LNA **Y2** and complementary DNA **D2** (Figures 8 and S8 and S9, Supporting Information)[29] exhibited similar key features as **W2**:**D2**, i.e., intercalation of the pyrene moiety and efficient $\pi-\pi$ overlapping with flanking base pairs, similar sugar puckers and glycosidic torsion angles for $\mathbf{X_5/Y_5}$ and $\mathbf{A_6}$, and unwinding of the duplex and widening of the grooves.[29] Two minor structural differences observed with PyAc-α-L-amino-LNA duplex **Y2**:**D2** (Figures 8 and S9, Supporting Information) relative to **W2**:**D2** (Figure 7) or **X2**:**D2** (Figures 8 and S8, Supporting Information) included increased stacking interactions with $\mathbf{T_{13}}$ and $\mathbf{A_{14}}$ and an altered orientation of the pyrene moiety, i.e., $H3_{py}$ and $H4_{py}$ of monomer **Y** face the major groove while facing the minor groove in **W2**:**D2** and **X2**:**D2** (Figure S10, Supporting Information).[29]

The binding mode of the pyrene moiety of PyBu-α-L-amino-LNA was expected to be more ambiguous because (a) **Z1**−**Z5** exhibited lower increases in thermal affinity toward DNA complements in particular (Table 1), (b) **Z2** displayed markedly improved mismatch discrimination relative to PyMe/PyCO/PyAc-α-L-amino-LNA (Table 3), and (c) more subtle hybridization-induced bathochromic shifts of pyrene absorption maxima were observed (Table 6). In full agreement with these biophysical observations, molecular modeling suggested at least two different binding modes. An intercalated binding mode was observed that exhibited the hallmarks described above for **W2**-**Y2**:**D2** (Figure S11, Supporting Information). The model structure suggested that the long and relatively bulky butanoyl linker of PyBu-α-L-amino-LNA monomer **Z** (a) reduced $\pi-\pi$ overlap between the pyrene and the nucleobase moieties of $\mathbf{Z_5}$ and $\mathbf{A_6}$ to a minimum, while increasing overlap with $\mathbf{T_{13}}$ and $\mathbf{A_{14}}$, (b) was wedged into the duplex core in between $\mathbf{Z_5}$ and $\mathbf{A_6}$ to locally perturb the duplex and introduce a kink, and (c) oriented the pyrene moiety with the $H3_{pyr}$ and $H4_{pyr}$ sides facing the major groove (Figure S10, Supporting Information).[29]

The second binding mode is more in line with biophysical observations; the pyrene moiety is located at the floor of the major groove and is involved in nonspecific contacts with the Hoogsteen faces of $\mathbf{A_6}$, $\mathbf{C_{11}}$, $\mathbf{A_{12}}$, and $\mathbf{T_{13}}$ (Figures 8 and S12, Supporting Information).[29] Minor groove binders conjugated to ONs are known to increase the strength and specificity of hybridization.[45,46] By analogy, major groove binding of the pyrene moiety of monomer **Z** may explain the observed increased mismatch discrimination of **Z2** (Table 3). Thus, biophysical characterization and computer simulations indicate that PyBu-α-L-LNA may stabilize duplexes with DNA/RNA complements by a wider variety of binding modes than PyMe/PyCO/PyAc-α-L-LNA exhibiting shorter linkers between the bicyclic skeleton and pyrene moiety.

Closer scrutiny of the molecular arrangement in PyMe/PyCO/PyAc-α-L-amino-LNA monomers **W**−**Y** reveals that the at-

(39) (a) Korshun, V. A.; Stetsenko, D. A.; Gait, M. J. *J. Chem. Soc. Perkin Trans. 1* **2002**, 1092–1104. (b) Dioubankova, N. N.; Malakhov, A. D.; Stetsenko, D. A.; Gait, M. J.; Volynsky, P. E.; Efremov, R. G.; Korshun, V. A. *ChemBioChem* **2003**, *4*, 841–847. (c) Kalra, N.; Babu, B. R.; Parmar, V. S.; Wengel, J. *Org. Biomol. Chem.* **2004**, *2*, 2885–2887. (d) Donho, C.; Saito, I. *ChemBioChem* **2005**, *6*, 1075–1081.

(40) Nakamura, M.; Fukunaga, Y.; Sasa, K.; Ohtoshi, Y.; Kanaori, K.; Hayashi, H.; Nakano, H.; Yamana, K. *Nucleic Acids Res.* **2005**, *33*, 5887–5895.

(41) Dougherty, G.; Pilbrow, J. R. *Int. J. Biochem.* **1984**, *16*, 1179–1192.

(42) Okamoto, A.; Kanatani, K.; Saito, I. *J. Am. Chem. Soc.* **2004**, *126*, 4820–4827.

(43) (a) Wang, A. H.-J.; Ughetto, G.; Quigley, G. J.; Rich, A. *Biochemistry* **1987**, *26*, 1152–1163. (b) Spielmann, H. P.; Wemmer, D. E.; Jacobsen, J. P. *Biochemistry* **1995**, *34*, 8542–8553. (c) Gallego, J.; Reid, B. R. *Biochemistry* **1999**, *38*, 15104–15115. (d) Mukherjee, A.; Lavery, R.; Bagchi, B.; Hynes, J. T. *J. Am. Chem. Soc.* **2008**, *130*, 9747–9755.

(44) The following definitions of torsion angles are used: χ (O4′−C1′−N1−C2 or O4′−C1′−N9−C4 for pyrimidines or purines, respectively). The pseudorotation phase angle P is given as $\tan P = (\nu_4 + \nu_1 - \nu_3 + \nu_0)/[2\nu_2(\sin 36° + \sin 72°)]$, where ν_0 (C4′−O4′−C1′−C2′), ν_1 (O4′−C1′−C2′−C3′), ν_2 (C1′−C2′−C3′−C4′), ν_3 (C2′−C3′−C4′−O4′), and ν_4 (C3′−C4′−O4′−C1′). For further information see: Saenger, W. *Principles of Nucleic Acid Structure*; Springer-Verlag: Berlin, 1984.

(45) Afonina, I.; Kutyavin, I.; Lukhtanov, E.; Meyer, R. B.; Gamper, H. *Proc. Natl. Acad. Sci. U.S.A.* **1996**, *93*, 3199–3204.

(46) Kutyavin, I. V.; Afonina, I. A.; Mills, A.; Gorn, V. V.; Lukhtanov, E. A.; Belousov, E. S.; Singer, M. J.; Walburger, D. K.; Lokhov, S. G.; Gall, A. A.; Dempcy, R.; Reed, M. W.; Meyer, R. B.; Hedgpeth, J. *Nucleic Acids Res.* **2000**, *28*, 655–661.

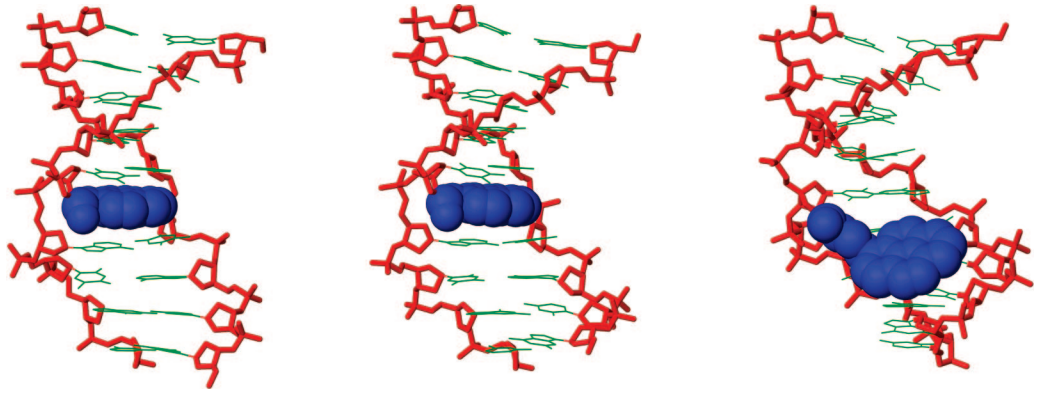

FIGURE 8. Side view representations of the lowest energy structures of **X2**:**D2**, **Y2**:**D2**, and **Z2**:**D2** (nonintercalated binding mode), respectively. Coloring scheme as in Figure 3 except that pyrene moieties are shown in blue.

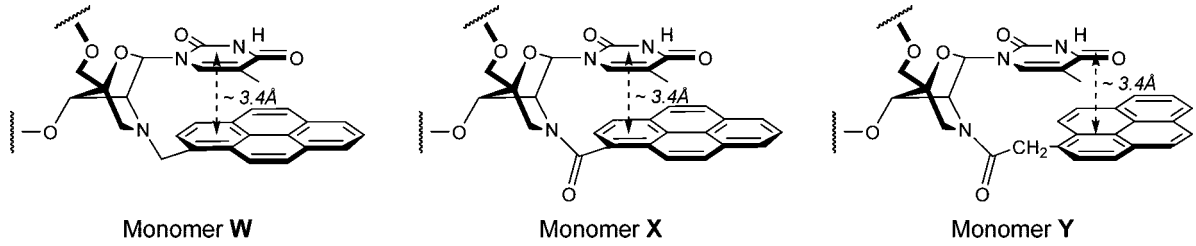

FIGURE 9. Illustration of directed positioning of pyrene moieties in the duplex core by N2′-functionalized 2′-amino-α-L-LNA.

tachment points of the nucleobase and pyrene moieties (i.e., C1′ and N2′, respectively) are efficiently locked relative to each other (Figure 9) as a consequence of the 2-oxo-5-azabicyclo[2.2.1]heptane skeleton. This, in concert with the short linker between the bicyclic skeleton and pyrene moiety and the strength of $\pi-\pi$ stacking in aqueous environments, de facto directs the pyrene moiety of monomers **W**−**Y** into the duplex core to facilitate intercalation. This molecular arrangement leads to $\pi-\pi$ stacking with the $\mathbf{T_5}$:$\mathbf{A_{14}}$ and $\mathbf{A_6}$:$\mathbf{T_{13}}$ base pairs and a reduction in buckle and propeller twist fluctuation in this nucleotide step (results not shown) to form a highly stablilized duplex segment. The observed thermodynamic data for PyMe/PyCO/PyAc-α-L-amino-LNA are in agreement with this preorganized binding mode of the pyrene as favorable entropic components were identified as important factors for duplex stabilization (Table 5). Desolvation upon intercalation of the highly apolar pyrene moiety is also likely to result in additional favorable entropic contributions upon duplex formation. Since the observed modeling structures of **W2**:**D2**, **X2**:**D2**, and **Y2**:**D2** are very similar, it is likely that differential solvation of the single-stranded probes or of their duplexes with DNA/RNA complements accounts for the observed differences in thermal affinity toward nucleic acid targets. For example, less pronounced desolvation of PyCO-α-L-amino-LNA **X2** relative to PyMe-α-L-amino-LNA **W2** upon hybridization to complementary DNA may account for less favorable entropy (fewer water molecules free upon hybridization) and more favorable enthalpy (formation of hydrogen bonds with surrounding water molecules).

Conclusion

Herein we demonstrate that the 2-oxo-5-azabicyclo-[2.2.1]heptane skeleton of 2′-amino-α-L-LNA, in concert with short linkers, directs intercalators appended to the N2′-position very effectively to the nucleic acid cores. Consequently, dramatic increases in thermal affinity toward DNA complements of up to +19.5 °C per modification are observed. Directed positioning of intercalators inside nucleic acid duplex cores has many potential interesting applications within nucleic acid based diagnostics, therapeutics, and nanotechnology,[47] including detection of DNA/RNA complements and/or single nucleotide polymorphisms by fluorescence,[25b,30a,48−50] study of charge transfer processes,[51] positioning of metal ions within nucleic acid duplex cores,[52,53] or development of artificial nucleases.[54] Unlike previously reported building blocks, N2′-intercalator-functionalized 2′-amino-α-L-LNA effectively combines high-affinity hybridization with DNA complements and precise positioning of intercalators in nucleic acid duplexes. We propose N2′-intercalator-modified 2′-amino-α-L-LNA monomers as highly valuable monomers for established and emerging DNA-targeting applications.

Experimental Section

(1*S*,3*R*,4*S*,7*R*)-1-(4,4′-Dimethoxytrityloxymethyl)-5-ethyl-7-hydroxy-3-(thymin-1-yl)-2-oxa-5-azabicyclo[2.2.1]heptane, 2S. Amino alcohol **1** (0.40 g, 0.70 mmol) was coevaporated with anhydrous 1,2-dichloroethane (2 × 8 mL) and dissolved in anhydrous 1,2-dichloroethane (8 mL). To this were added $NaBH(OAc)_3$ (230 mg, 1.09 mmol) and CH_3CHO (44 μL, 0.78 mmol), and after the reaction mixture was stirred at room temperature for 40 h, it was diluted with EtOAc (35 mL) and washed with saturated aqueous $NaHCO_3$ (2 × 15 mL). The organic phase was evaporated to

(47) Persil, Ö.; Hud, N. V. *Trends Biotechnol.* **2007**, *25*, 433–436.
(48) Wilson, J. N.; Kool, E. T. *Org. Biomol. Chem.* **2006**, *4*, 4265–4274.
(49) Köhler, O.; Jarikote, D. V.; Seitz, O. *ChemBioChem* **2005**, *6*, 69–77.
(50) Benvin, A. L.; Creeger, Y.; Fisher, G. W.; Ballou, B.; Wagonner, A. S.; Armitage, B. A. *J. Am. Chem. Soc.* **2007**, *129*, 2025–2034.
(51) Shao, F.; Augustyn, K.; Barton, J. K. *J. Am. Chem. Soc.* **2005**, *127*, 17445–17452.
(52) Clever, G. H.; Kaul, C.; Carell, T. *Angew. Chem., Int. Ed.* **2007**, *46*, 6226–6236.
(53) Tanaka, K.; Shionoya, M. *Coord. Chem. Rev.* **2007**, *251*, 2732–2742.
(54) Nakano, S-I.; Uotani, Y.; Uenishi, K.; Fujii, M.; Sugimoto, N. *J. Am. Chem. Soc.* **2005**, *127*, 518–519.

dryness, and the resulting residue was purified by silica gel column chromatography (0−5% *i*-PrOH in CH_2Cl_2, v/v) to afford nucleoside **2S** (200 mg, 48%). $R_f = 0.5$ (10% MeOH in CH_2Cl_2, v/v); MALDI-HRMS *m/z* 622.2524 ($[M + Na]^+$, $C_{34}H_{37}N_3O_7Na^+$ calcd 622.2522); ^{1}H NMR (DMSO-d_6)[55] δ 11.26 (s, 1H, ex, NH), 7.49 (s, 1H, H-6), 7.21−7.44 (m, 9H, Ar), 6.87−6.92 (d, 4H, $J = 8.8$ Hz, Ar), 5.91 (d, 1H, $J = 1.5$ Hz, H-1′), 5.70 (d, 1H, ex, $J = 3.5$ Hz, 3′-OH), 4.31 (d, 1H, $J = 3.5$ Hz, H-3′), 3.74 (s, 6H, 2 × CH_3O), 3.19−3.30 (m, 4H, H-2′, 2 × H-5′, H-5″), 2.64−2.83 (m, 3H, CH_2CH$_3$, H-5″), 1.83 (s, 3H, CH_3Ar), 0.82 (t, 3H, $J = 7.3$ Hz, CH_3). ^{13}C NMR (DMSO-d_6) δ 163.8, 158.0, 150.3, 144.8, 137.4, 135.4, 135.3, 129.7, 127.8, 127.6, 126.6, 113.1, 105.9, 90.0, 85.0, 74.4, 65.4, 60.8, 58.3, 54.9, 49.5, 14.8, 12.2. Anal. Calcd for $C_{34}H_{37}N_3O_7$: C, 68.10; H, 6.22; N, 7.01. Found: C, 67.96; H, 6.37; N, 6.54. Calcd with 1/8 *i*-PrOH: C, 68.00; H, 6.31; N, 6.92.

(1*S*,3*R*,4*S*,7*R*)-1-(4,4′-Dimethoxytrityloxymethyl)-7-hydroxy-5-(pyren-1-yl)carbonyl-3-(thymin-1-yl)-2-oxa-5-azabicyclo[2.2.1]heptane, 2X. 1-Pyrenylcarboxylic acid (162 mg, 0.65 mmol), *O*-(7-Azabenzotriazole-1-yl)-*N*,*N*,*N*′,*N*′-tetramethyluronium hexafluorophosphate (HATU, 183 mg, 0.48 mmol), and *N*,*N*′-diisopropylethylamine (0.19 mL, 1.1 mmol) were dissolved in anhydrous DMF (4.2 mL), and the mixture was allowed to stir for 6 h at room temperature. To this was added a solution of nucleoside **1** (0.25 g, 0.44 mmol), which had been dried by coevaporation with anhydrous toulene (2 × 10 mL) ahead of time, dissolved in anhydrous DMF (4.2 mL). After stirring at room temperature for 12 h, the reaction mixture was diluted with CH_2Cl_2 (50 mL) and washed with saturated aqueous $NaHCO_3$ (10 mL) and H_2O (4 × 10 mL). The aqueous phase was back-extracted with CH_2Cl_2 (2 × 30 mL), the combined organic phase was evaporated to dryness, and the resulting crude residue was adsorbed on silica gel and purified by silica gel column chromatography (0−4% MeOH in CH_2Cl_2, v/v) to afford a rotameric mixture (∼1:1.4 by ^{1}H NMR) of nucleoside **2X** as a white solid material (0.32 g, 90%). $R_f = 0.2$ (50% acetone in petroleum ether, v/v), MALDI-HRMS *m/z* 822.2786 ($[M + Na]^+$, $C_{49}H_{41}N_3O_8 \cdot Na^+$ calcd 822.2746; selected signals ^{1}H NMR (DMSO-d_6)[56] δ 6.47 (d, 1H, ex, $J = 3.7$ Hz, 3′-OH$_B$), 6.43 (d, 1.4H, ex, $J = 3.8$ Hz, 3′-OH$_A$), 6.25 (s, 1H, H-1′$_B$), 5.80 (s, 1.4H, H-1′$_A$), 4.79 (d, 1H, $J = 3.7$ Hz, H-3′$_B$), 4.56 (d, 1.4H, $J = 3.8$ Hz, H-3′$_A$), 2.05 (s, 4.2H, CH$_{3\text{-}A}$), 1.92 (s, 3H, CH$_{3\text{-}A}$); ^{13}C NMR (DMSO-d_6) δ 169.6, 169.5, 164.2, 163.8, 158.3, 158.1, 150.3, 149.6, 144.8, 144.6, 135.4, 135.3, 135.2, 135.1, 134.6, 131.6, 131.4, 130.7, 130.5, 130.25, 130.18, 129.9, 129.8, 128.8, 128.53, 128.46, 128.1, 127.9, 127.8, 127.7, 127.3, 127.2, 126.92, 126.86, 126.8, 126.4, 126.2, 126.1, 125.9, 124.9, 124.5, 124.2, 123.8, 123.7, 123.6, 113.4, 113.2, 109.1, 108.5, 89.0, 88.8, 86.0, 85.6, 85.4, 72.4, 71.5, 64.9, 62.0, 60.3, 59.6, 55.1, 55.0, 53.9, 52.1, 12.6, 12.5. Anal. Calcd for $C_{49}H_{41}N_3O_8 \cdot 1H_2O$: C, 71.96; H, 5.30; N, 5.14. Found: C, 71.63; H, 4.95; N, 4.77.

(1*S*,3*R*,4*S*,7*R*)-7-[2-Cyanoethoxy(diisopropylamino)phosphinoxy]-1-(4,4′-dimethoxytrityloxymethyl)-5-ethyl-3-(thymin-1-yl)-2-oxa-5-azabicyclo[2.2.1]heptane, 3S. Nucleoside **2S** (190 mg, 0.32 mmol) was coevaporated with anhydrous 1,2-dichloroethane (2 × 5 mL) and dissolved in a mixture of anhydrous Et$N(i\text{-}Pr)_2$ in CH_2Cl_2 (2 mL, 20%, v/v). To this was added 2-cyanoethyl *N*,*N*′-(diisopropyl)phosphoramidochloridite (0.14 mL, 0.63 mmol), and the reaction mixture was stirred at room temperature for 1 h, whereupon it was diluted with CH_2Cl_2 (20 mL). The organic phase was washed with saturated aqueous $NaHCO_3$ (10 mL), and the aqueous phase was back-extracted with CH_2Cl_2 (25 mL). The combined organic phase was evaporated to dryness, and the resulting residue was purified by silica gel column chromatography (0−50% EtOAc in petroleum ether, v/v) to afford amidite **3S** (160 mg, 63%) as a white solid material. $R_f = 0.5$ (70% EtOAc in petroleum ether, v/v); MALDI-HRMS *m/z* 822.3636 ($[M + Na]^+$, $C_{43}H_{54}N_5O_8P \cdot Na^+$ calcd 822.3602); ^{31}P NMR (CH_3CN + DMSO-d_6) δ 149.8, 147.9.

(1*S*,3*R*,4*S*,7*R*)-7-[2-Cyanoethoxy(diisopropylamino)phosphinoxy]-1-(4,4′-dimethoxytrityloxymethyl)-5-(pyren-1-yl)carbonyl-3-(thymin-1-yl)-2-oxa-5-azabicyclo[2.2.1]heptane, 3X. Nucleoside **2X** (0.31 g, 0.39 mmol) was dried by coevaporation with anhydrous 1,2-dichloroethane (2 × 5 mL) and dissolved in anhydrous CH_2Cl_2 (10 mL). To this were added *N*,*N*′-diisopropylammonium tetrazolide (112 mg, 0.66 mmol) and bis(*N*,*N*′-diisopropylamino)-2-cyanoethoxyphosphine (0.21 mL, 0.66 mmol), and the reaction mixture was stirred at room temperature for 12 h, whereupon it was diluted with CH_2Cl_2 (20 mL) and washed with saturated aqueous $NaHCO_3$ (10 mL) and brine (10 mL). The aqueous phase was back-extracted with CH_2Cl_2 (30 mL), the combined organic phase was evaporated to dryness, and the resulting residue was purified by silica gel column chromatography (0−50% acetone in petroleum ether, v/v) to afford amidite **3X** as a white solid material (276 mg, 71%). $R_f = 0.5$ (50% acetone in petroleum ether, v/v); MALDI-HRMS *m/z* 1022.3864 ($[M + Na]^+$, $C_{58}H_{58}N_5O_9PNa^+$ calcd 1022.3852; ^{31}P NMR (CH_3CN + DMSO-d_6) δ 154.2, 153.8, 153.3, 151.9.

Protocol for Synthesis of ONs. ONs containing 2′-amino-α-L-LNA monomers **Q**−**Z** (see Figure 1 for structures) were synthesized on a 0.2 μmol scale using succinyl-linked LCAA-CPG (long chain alkyl amine controlled pore glass) columns with a pore size of 500 Å on an automated DNA synthesizer. Synthesis of α-L-LNA and 2′-amino-α-L-LNA was performed as previously described.[15b,24b] For the incorporation of the N2′-functionalized 2′-amino-α-L-LNA monomers (**S**−**Z**), standard procedures were used, i.e., trichloroacetic acid in CH_2Cl_2 as a detrytilation reagent; 0.25 M 4,5-dicyanoimidazole (DCI) in CH_3CN as activator; acetic anhydride in THF as cap A solution; 1-methylimidazole in THF as cap B solution, and 0.02 M iodine in H_2O/pyridine/THF as the oxidizing solution. Extended coupling times used for phosphoramidites **3S** (10 min), **3V** (10 min), **3W** (30 min), **3Y** (30 min), **3X** (30 min), and **3Z** (15 min) using 1*H*-tetrazole as catalyst resulted in stepwise coupling yields of ∼99% for monomers **S**, **V**, **X**, **Y**, and **Z** and ∼95% for monomer **W**. Coupling yields were determined by trityl monitoring. Removal of the nucleobase protecting groups of ONs and cleavage from solid support was accomplished using standard conditions (32% aqueous ammonia for 12−16 h at 55 °C). Unmodified DNA and RNA strands were obtained from commercial suppliers and, if necessary, further purified as described below.

Purification of all modified ONs (till minimum 80% purity) was performed by two different methods: (a) if overall yield >90%, precipitation of crude ONs (DMT-OFF, absolute EtOH, −18 °C, 12−16 h, followed by washing with absolute EtOH (2 × 300 μL), or (b) purification of the ONs (DMT-ON) by RP-HPLC using the system described below, followed by detritylation (80% aqueous AcOH, 20 min, room temperature) and precipitation/washing as outlined above. Purification of crude ONs (DMT-ONs) was performed using a HPLC system equipped with an Xterra MS C18 (10 μm, 7.8 mm × 10 mm) precolumn and an Xterra MS C18 (10 μm, 7.8 mm × 150 mm) column using the representative gradient protocol depicted in Table S1, Supporting Information. The composition of all synthesized ONs were verified by MALDI-MS analysis (Table S3, Supporting Information) recorded in negative ion mode using 3-hydroxypicolinic acid as a matrix, whereas the purity (>80%) was verified by ion-exchange HPLC system equipped with a Dionex PA100 column (4 × 250 mm) at pH 8 using the representative protocol shown in Table S2, Supporting Information.

Protocol for Thermal Denaturation Studies. Concentrations of ONs were estimated using the following extinction coefficients for DNA (OD/μmol): G (12.01), A (15.20), T (8.40), C (7.05); for RNA (OD/μmol): G (13.70), A (15.40), U (10.00), C (9.00); and for pyrene (22.4). ONs (1.0 μM each strand) were thoroughly mixed, denatured by heating, and subsequently cooled to the starting temperature of the experiment. Quartz optical cells with a path

(55) Assignments of ^{1}H NMR signals of H5′ and H5″ (and of the corresponding ^{13}C signals) may in principle be interchanged.

(56) The integral of the H1′ signal of the least predominant rotamer (termed B) is set to 1.0.

length of 1.0 cm were used. Thermal denaturation temperatures (T_m values/°C) were measured on a UV−vis spectrometer equipped with a Peltier temperature programmer and determined as the maximum of the first derivative of the thermal denaturation curve (A_{260} vs temperature) recorded in medium salt buffer (T_m buffer; 100 mM NaCl, 0.1 mM EDTA and pH 7.0 adjusted with 10 mM NaH_2PO_4/5 mM Na_2HPO_4). For studies evaluating the dependence of T_m on ionic strength, T_m values were also determined in low and high salt buffers (composition as for medium salt buffer except that 0 and 700 mM NaCl were used, respectively). The temperature of the denaturation experiments ranged from at least 15 °C below T_m to 20 °C above T_m (although not below 1 °C). A temperature ramp of 1.0 °C/min was used in all experiments. Reported thermal denaturation temperatures are an average of two measurements within ±1.0 °C.

Protocol for Determination of Thermodynamic Parameters. Thermodynamic parameters were obtained by analysis of the melting curves used to determine T_m values assuming bimolecular reactions and two-state equilibrium hypothesis, using software accompanying the utilized UV−vis spectrometer. The graphs of ln K_a (affinity constant) as a function of $1/T$ were approximated with straight lines facilitating parameter determination (ΔG, ΔH, and ΔS, Tables 4 and 5). Quality of the baseline permitting, thermodynamic parameters for two melting curves per investigated duplex were determined, and an average value was listed. The changes in Gibbs free energy, ΔG, were determined at temperatures close to the T_m value of the investigated duplexes to minimize errors ($T = 298$ K).

Acknowledgment. We greatly appreciate financial support from Idaho NSF EPSCoR, the BANTech Center at the University of Idaho, a University of Idaho Research Office and Research Council Seed Grant, NIH Grant P20 RR016448 from the COBRE Program of the National Center for Research Resources, and The Danish National Research Foundation. The Nucleic Acid Center is funded by the Danish National Research Foundation for studies on nucleic acid chemical biology. The Ph.D. school Nucleic Acid Based Drug Design (NAC DRUG) supported by the Danish Agency for Science Technology and Innovation is gratefully acknowledged. The Hrdlicka research team is thanked for proofreading of the manuscript preparation.

Supporting Information Available: General experimental section; experimental section for synthesis of nucleosides **2** and **3** (**V/W/Y/Z**-series); copies of ^{1}H NMR, ^{13}C NMR, ^{31}P NMR, ^{1}H−^{1}H COSY and/or ^{1}H−^{13}C HETCOR spectra for all novel nucleosides; protocols for RP-HPLC and ion-exchange HPLC purification of ONs; MALDI-MS of synthesized ONs (Table S3); representative thermal denaturation curves (Figure S1); T_m values of N2′-functionalized 2′-amino-α-L-LNA at various ionic strengths (Table S4); discussion of sequence dependent variation of T_m values; DNA-selectivity of N2′-functionalized 2′-amino-α-L-LNA (Table S5); thermodynamic data for **B1**−**B5** and full discussion thereof (Table S6); protocol for acquisition and listing of additional CD spectra (Figure S2); protocol for molecular modeling studies; additional molecular modeling structures (Figures S3−S9, S11, and S12), illustration of intercalation (Figure S10); pseudorotational phase angle P and glycosidic torsion angle χ observed in simulated duplexes (Tables S7 and S8). This material is available free of charge via the Internet at http://pubs.acs.org.

JO802037V